DESY 04-106

DESY 04-106

arXiv:hep-ph/0406273 v1 24 Jun 2004

$\gamma^*\,\gamma^*$ SCATTERING VIA SECONDARY REGGEON EXCHANGE IN QCD

JOCHEN BARTELS

II. Institut für Theoretische Physik, Universität Hamburg
Luruper Chaussee 149, 22761 Hamburg, Germany
bartels@mail.desy.de

MICHAEL LUBLINSKY

DESY Theory Group, DESY
Notkestr. 85, 22607 Hamburg, Germany
lublinm@mail.desy.de

We summarize the results on the high energy behavior of quark-antiquark exchange in $\gamma^*\gamma^*$ elastic scattering. The ladder diagrams, summed in the double logarithmic approximation, provide a perturbative QCD model for secondary reggeon exchange.

Keywords: QCD; secondary reggeon; quark ladder.

1. Introduction

$\gamma^*\,\gamma^*$ collisions at high energies provide a unique laboratory for testing asymptotic properties of perturbative QCD. The virtuality of the photons justifies the use of perturbative QCD, and modern electron positron colliders (LEPII, a future linear collider NLC) allow to measure the total cross section of $\gamma^*\,\gamma^*$ scattering at energies where asymptotic predictions of perturbative QCD can be expected to set in. The dominant contribution to the process is given by the BFKL Pomeron [1] which gives rise to a cross section strongly rising with energy $\sigma_{total}^{\gamma^*\gamma^*} \sim s^{\alpha_P(0)}$. Here $\alpha_P(0)$ is the Pomeron intercept which, in leading order and for realistic values of the photon virtualities, lies in the region $\alpha_P(0) \simeq 0.3 - 0.5$.

There is little doubt that the pomeron will dominate at very high energies, and it is expected to be a main contribution at any future linear collider. At present, however, the only source for experimental data on photon photon collisions is LEP [2,3]. These data are at energies which cannot be considered as asymptotically large, and it has become clear that at LEP energies, the cross section is not yet dominated by the pomeron [4,5,6,7,8,9]. The data rather indicate the necessity to include, in the theoretical description, several corrections. Perturbative corrections are due to the quark box (the first α_s correction was computed in Ref. [10]). Nonperturbative contributions include, in particular, the soft Pomeron exchange.

Another class of corrections are due to the exchange of secondary reggeons: f_0 (flavor singlet) or A_0, A_2 (flavor nonsinglet) [6,7,8]. In hadron scattering, secondary reggeons denote the exchange of mesons and are of nonperturbative nature. In

virtual $\gamma^*\gamma^*$ scattering, however, we may expect that such secondary exchange may become accessible to a perturbative analysis: similar to BFKL exchange. The hard scale at both ends of the exchanged reggeon provides a justification for using pQCD, provided the photon virtualities are sufficiently large. If so, meson exchange will be modeled by the exchange of $q\bar{q}$ ladders [11], and the prediction for the energy dependence may be tested in the corrections to BFKL exchange in $\gamma^*\gamma^*$ scattering.

Technically speaking, there is a striking difference between gluon exchange in the BFKL calculations and quark-antiquark exchange: the appearance of double logarithms [12,13]. As result of this, the intercept of the $q\bar{q}$-system is of the order $\omega_0^{q\bar{q}} = \sqrt{const\ \alpha_s}$ (as opposed to $\omega_0^{BFKL} = const\ \alpha_s$ in the single logarithmic high energy behavior of the BFKL Pomeron), and its numerical value can be expected to be large. In fact, for $q\bar{q}$ scattering it is known [11] that the cross section goes as $\sim s^{\omega_0 - 1}$ with $\omega_0 = \sqrt{2\,\alpha_s\,C_F/\pi} \simeq 0.5$. It is remarkable that this intercept obtained in pQCD is very close to the nonperturbative one known from Regge phenomenology. This observation justifies the hope that a perturbative calculation of $q\bar{q}$ exchange in $\gamma^*\gamma^*$ scattering, in fact, might be a reasonable model for the exchange of secondary reggeons. In this model, pQCD then allows to make an absolute prediction of the magnitude of these corrections.

Connected with the appearance of double logarithms in $q\bar{q}$ exchange is the role of the infrared region. The ladder graphs that have to be summed are infrared finite. However, the comparison with the BFKL approximation leads us to expect that there are contribution from small momenta which, although not giving rise to infrared divergencies, are not believable. In BFKL, this infrared region is reached by diffusion in $\ln k_t^2$, i.e. even at large photon virtualities Q^2 where pQCD is well-justified, the BFKL prediction becomes unreliable when $\ln s/Q^2$ becomes of the order $\ln^2 Q^2/\mu_0^2$ (where μ_0^2 denotes the infrared momentum scale where pQCD becomes unreliable). The double logs in $q\bar{q}$ exchange do not allow for diffusion; the region of validity of the pQCD analysis, therefore, is different and needs to be investigated. Existing studies of fermion-antifermion exchange have never touched this question. $\gamma^*\gamma^*$ scattering appears to be a natural candidate for addressing this question.

In Ref. [14] we have performed a detailed study of the high energy behavior of quark-antiquark exchange in $\gamma^*\gamma^*$ scattering in the double logarithmic approximation. Three different approaches were exploited in Ref. [14]. Below we will outline only one of them based on a Bethe-Salpeter equation for a sum of Feynman diagrams. The other two methods are based on a Mellin space representation of the scattering amplitude. The first one uses the infrared evolution equation (IREE) for a partial wave [13]. A third way of handling the quark-antiquark exchange utilizes a notion of the reggeon Green's function, which has been described in Refs. [18,19]. In Ref. [14] all three methods were shown to agree with each other.

In this letter we present a brief summary of our results. We skip most of the technical details of our calculations, and we will only outline the way the results are obtained. Our main emphasis will be on the physical results.

2. Integral Equation

We start from the lowest order diagrams for the scattering amplitude $T^{\gamma^*\gamma^*}$ of the elastic $\gamma^*\gamma^*$ scattering process. We consider forward direction $t = 0$ only, and for simplicity we first take the virtualities of all external photons to be equal. The exact computation of the quark box can be found in Ref.[20]; we restrict ourselves to the high energy behavior. The lowest order consists of the three fermion-loop diagrams (Fig. 1, a - c); however, at high energies the diagram (c) does not contribute to the leading double-logarithmic behavior.

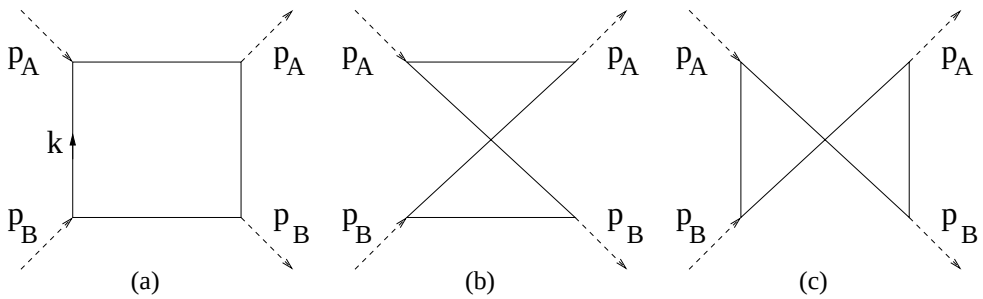

Fig. 1. The Born level diagrams.

The calculations below are done using the Feynman gauge. Our method of extracting the double-logs is close to the original paper [12]. With the notation (Fig. 1)

$$p_A^2 = -Q^2\,; \quad p_B^2 = -Q^2\,; \quad (p_A + p_B)^2 = s\,; \quad x = Q^2/s\,. \quad . \qquad (1)$$

and the Sudakov decomposition $k = \beta q - \alpha p + k_\perp$ (with $k_\perp^2 = -\vec{k}^2$) the light cone vectors p, q are defined through

$$p_A = p - x\,q\,; \qquad p_B = q - x\,p\,; \qquad p^2 = q^2 = 0\,; \qquad 2\,(p\,q) = s\,. \qquad (2)$$

The scattering of the longitudinally polarized photons has additional energy suppression, and we will consider transverse polarizations only. Transverse polarization vectors are defined by $\epsilon_\pm^\mu = \frac{1}{\sqrt{2}}\,(0, 1, \pm i, 0)$.

In order to find a double-logarithmic contribution of the quark loop we need to find, in the trace expression in the numerator, terms proportional the leading power of s and to $k_\perp^2$. For the numerator of the planar box diagram we obtain:

$$trace \approx 2\,s\,k_\perp^2\,\tau_{TT}\,; \qquad \tau_{TT} = 4\,N_c\,\alpha_{em}^2\,F_{ns}\;\epsilon(A)\cdot\epsilon(A')\;\epsilon(B)\cdot\epsilon(B'), \qquad (3)$$

where

$$F_{ns} = \sum_{quarks} e_q^4 - \frac{1}{N_f}\,(\sum_{quarks} e_q^2)^2 \qquad (4)$$

denotes the projection on the flavor nonsinglet t-channel (for the flavor group $SU(N_f)$), and e_q stands for the electric charge of the quark, measured in units of e. Diagram Fig. 1b will be obtained by simply substituting, at the end of our calculation, $s \to u$.

The analysis of the double logarithmic part of the integration region can be summarized as follows. The energies of the s-channel quark lines have to be positive; equivalently, the momentum fractions of the large incoming momenta range between x and 1. This leads to the limits:

$$x = \frac{Q^2}{s} < \alpha, \beta < 1 . \tag{5}$$

The momenta of the t-channel quark lines have to be space-like, i.e.

$$s\,\alpha\,\beta < \vec{k}^2 . \tag{6}$$

Combining these two conditions we are lead to

$$\frac{Q^4}{s} < \vec{k}^2 . \tag{7}$$

Furthermore, in order to justify the use of perturbation theory the virtualities of the t-channel quark lines have to be larger than the infrared cutoff which we denote by μ_0^2:

$$\mu_0^2 < \vec{k}^2 . \tag{8}$$

Now two possibilities arise. For sufficiently large photon virtualities, Q^2, we have $\mu_0^2 < \frac{Q^4}{s}$, i.e. in the entire double logarithmic region the momentum scale of the exchanged quark lines is above the infrared cutoff. If, on the other hand, the energy s grows and the lower cutoff, $\frac{Q^4}{s}$, enters the infrared region $\frac{Q^4}{s} < \mu_0^2$, we have to impose a further restriction on the transverse momentum integration: $\frac{Q^4}{s} < \mu_0^2 < \vec{k}^2$. We therefore define, for the external kinematic variables s and Q^2, two different regions which we denote by '+' and '−':

$$I^+ : \ \mu_0^2 < \frac{Q^4}{s} ; \qquad\qquad I^- : \ \frac{Q^4}{s} < \mu_0^2 . \tag{9}$$

The '+' region defines the hard domain where the result is infrared insensitive. Below we will find that, in this region, the amplitude in fact has no dependence on μ_0^2 at all.

The integrals are performed in the following way. The α-integral is done by putting one of the s-channel quark lines, say the lowest one, on the mass shell. This integration sets $\alpha = x$. With the condition that

$$\vec{k}^2 < s\,\beta , \tag{10}$$

the other s-channel quark propagator provides the factor $1/\beta$, needed to make the β-integral logarithmic. The remaining integrals are:

$$\int_x^1 \frac{d\beta}{\beta} \int_{max(\mu_0^2,\,\beta\,Q^2)}^{\beta\,s} \frac{dk^2}{k^2} , \tag{11}$$

The first energy log then comes from the β integration; its limits follow from (5). As to the remaining integral over the transverse momentum, it is the fermionic nature of the exchanged particles which provides, in the trace in the numerator, the additional k^2 factor and thus renders the momentum integral logarithmic. The upper limit of integration results from (10), whereas the lower one combines the two possibilities (7) and (8). If we are in the '+' region, we always have $\mu_0^2 < \beta Q^2$, and there is no μ_0-dependence. On the other hand, in the '-' region, we have to split the β region into two pieces and to perform, for each piece, the k integral separately.

The result for the planar box diagram in the two regions has the form

$$T_{box}^{\pm} = \tau_{TT} \left\{ \begin{array}{lll} \ln^2 \frac{s}{Q^2} & if & \mu_0^2 < \frac{Q^4}{s} \\ \ln^2 \frac{s}{Q^2} - \frac{1}{2}\left(\ln \frac{s}{Q^2} - \ln \frac{Q^2}{\mu_0^2}\right)^2 & if & \frac{Q^4}{s} < \mu_0^2 \end{array} \right\} . \tag{12}$$

In the second case, I^-, we see that we are cutting a piece of the phase space, i.e the result for I^- is smaller than for I^+. The nonplanar box in Fig. 1b is obtained by substituting $s \to u$, and in the sum of the two diagrams the obtained results stand for the even signature A_2 exchange. The total cross section for $\gamma^*\,\gamma^*$ (averaged over the incoming transverse helicities) follows from

$$\sigma^{\gamma^*\,\gamma^*} = \frac{1}{s}\, Im\, T \simeq \frac{1}{s}\, \frac{\pi\, \partial T}{\partial \ln s} \tag{13}$$

(with the last approximate equality being valid in the high energy approximation only) and has the form

$$\sigma_{Born}^{\gamma^*\,\gamma^*} = \tau_{TT}\, \pi \left\{ \begin{array}{lll} 2\, \ln \frac{s}{Q^2} & if & \mu_0^2 < \frac{Q^4}{s} \\ \ln \frac{s}{\mu_0^2} & if & \frac{Q^4}{s} < \mu_0^2 \end{array} \right\} . \tag{14}$$

It is not difficult to generalize this analysis to the case of unequal photon masses, Q_1^2 and Q_2^2. In this case the boundary of the hard domain will be determined from the equation $Q_1^2\, Q_2^2 = \mu_o^2\, s$.

We now turn to higher order corrections to the quark loop diagram. For the case of quark-quark scattering it has been shown [13] that the even signature amplitude is described by the QCD ladder diagrams. For our analysis we make use of the discussion given in [12,13,15,16,17].

From the trace expression in the numerator we obtain, for each i-th rung, a factor $k_i^2\, \lambda$ (with $\lambda = \frac{\alpha_s\, C_F}{2\, \pi}$). Thus each rung in the ladder brings in

$$\lambda \int \frac{d\, \beta_i}{\beta_i} \int \frac{d\, k_i^2}{k_i^2} . \tag{15}$$

Generalizing the above discussion of the double logarithmic phase space, one finds the following ordering conditions:

$$x < \beta_1 < \beta_2 < \ldots < \beta_{n-1} < \beta_n < 1 ,$$

$$Q^2 < \frac{k_n^2}{\beta_n} < \frac{k_{n-1}^2}{\beta_{n-1}} < \ldots < \frac{k_1^2}{\beta_1} < s .$$

In addition we require for each rung to satisfy $k_i^2 > \mu_0^2$.

Fig. 2 illustrates the Bethe-Salpeter type equation we are deriving for the sum of ladder diagrams. We simply remove the lower s-channel quark line coupling; in this way we obtain (up to an overall factor) the elastic amplitude A for the photon-quark scattering. $A(\beta,\, k^2) \,=\, \sum_n A_n$ where A_n denotes a contribution of n-rung diagram ($A_0 \,=\, 1$). The amplitudes A_n satisfies the following recurrence relation

$$A_n(\beta,\, k^2) \,=\, \lambda \int_{Q^2/s}^{\beta} \frac{d\beta'}{\beta'} \int_{max(\beta'\, k^2/\beta\, ,\, \mu_0^2)}^{\beta'\, s} \frac{dk'^2}{k'^2}\, A_{n-1}(\beta',\, k'^2)\,. \tag{16}$$

The limits of integration follow from the above kinematic ordering.

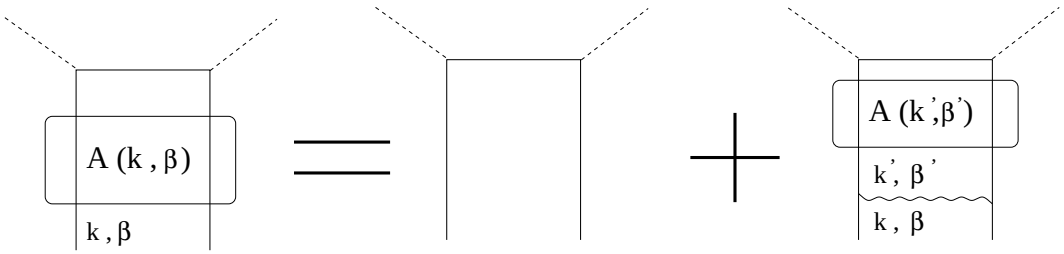

Fig. 2. The Bethe - Salpeter equation.

As in the case of the box diagram we have to distinguish between two regions I_A^+ and I_A^- defined as

$$I_A^+ :\quad \mu_0^2 \,<\, \frac{Q^2\, k^2}{\beta\, s}\,; \qquad\qquad I_A^- :\quad \frac{Q^2\, k^2}{\beta\, s} \,<\, \mu_0^2\,. \tag{17}$$

For the amplitudes A_n, the kinematics of the lower quark lines plays the same role as, in the case of the simple quark box, the lower external photon lines. The distinction between the two different regions makes it necessary to define two separate amplitudes, A^+ and A^-. The recurrence relation (16) expresses A_n^- in terms of A_{n-1}^+ and A_{n-1}^-, whereas A_n^+ only needs A_{n-1}^+ on the rhs. Taking the sum over n, we obtain the integral equations

$$A^+(\beta,\, k^2) \,=\, 1 \,+\, \lambda \int_{Q^2/s}^{\beta} \frac{d\beta'}{\beta'} \int_{\beta'\, k^2/\beta}^{\beta'\, s} \frac{dk'^2}{k'^2}\, A^+(\beta',\, k'^2) \tag{18}$$

and

$$\begin{aligned} A^-(\beta,\, k^2) \;&=\; 1 \,+\, \lambda \int_{Q^2/s}^{\beta} \frac{d\beta'}{\beta'} \int_{\beta'\, \mu_0^2/Q^2}^{\beta' s} \frac{dk'^2}{k'^2}\, A^+(\beta',\, k'^2) \\ &+\, \lambda \int_{Q^2/s}^{\beta\, \mu_0^2/k^2} \frac{d\beta'}{\beta'} \int_{\mu_0^2}^{\beta'\, \mu_0^2 s/Q^2} \frac{dk'^2}{k'^2}\, A^-(\beta',\, k'^2) \end{aligned} \tag{19}$$

$$+\,\lambda\int_{\beta\,\mu_0^2/k^2}^{\beta}\frac{d\beta'}{\beta'}\int_{\beta'\,k^2/\beta}^{s\,\beta'\,\mu_0^2/Q^2}\frac{dk'^2}{k'^2}\,A^-(\beta',\,k'^2).$$

Finally, the amplitudes T for the photon-photon scattering is obtained from A by subtracting the terms $A_0 = 1$, putting $k^2 = Q^2$ and $\beta = 1$ and restoring the overall normalization factor. Note that in this limit the regions I_A^+, I_A^- coincide with I^+ and I^- in (9). The full scattering amplitude is obtained by adding the twisted (with respect to $s \leftrightarrow u$ crossing) fermion loop. It is straightforward to generalize to the case of unequal photon masses [14]. We only quote the final result for the scattering amplitude:

$$T^{\pm}(Q_1^2,\,Q_2^2,\,s) \;=\; \left[A^{\pm}(1,Q_2^2)\;-\;1\right]\frac{\tau_{TT}}{\lambda}. \tag{20}$$

For the remainder of this letter, we shall discuss the general case of unequal photon masses.

3. Solution of the linear equations

The structure of the two equations, (18) and (19) defines our strategy: we first solve the equation for A^+, Eq. (18), and we then use the solution as an inhomogeneous term in the equation for A^-, Eq. (19). The main step is a choice of suitable variables.

In the infrared insensitive region I_A^+ where Eq. (18) holds we define the new variables:

$$\xi \;=\; \ln(\beta\,s/k^2)\,; \qquad\qquad \eta \;=\; \ln(\beta\,s/Q_1^2)\,.$$

In these new variables the equation (18) can be rewritten

$$A^+(\xi,\,\eta) \;=\; 1 \;+\; \lambda\int_0^{\eta}d\bar{\eta}\int_0^{\xi}d\bar{\xi}\,A^+(\bar{\xi},\,\bar{\eta})\,. \tag{21}$$

When differentiated twice Eq. (21) reduces to

$$\frac{d^2A^+}{d\xi\,d\eta} \;=\; \lambda\,A^+\,. \tag{22}$$

This is a wave equation in the light cone coordinates. Its solution is given by

$$A^+(\xi,\,\eta) \;=\; I_0\left(\sqrt{4\,\lambda\,\xi\,\eta}\right)\,. \tag{23}$$

In the infrared sensitive region I_A^- we have the integral equation (19) which couples the functions A^+ and A^-. Let us define a new variable:

$$\xi' \;=\; \xi \;-\; L_0\,; \qquad\qquad L_0 \;=\; \ln(Q_1^2/\mu_0^2)\,.$$

In the variables $(\xi',\,\eta)$ the solution of the equation (19) is following

$$A^-(\xi',\,\eta) \;=\; I_0\left(\sqrt{4\,\lambda\,(\xi'\;+\;L_0)\,\eta}\right)\;+\;\frac{\xi'}{\eta+L_0}\,I_2\left(\sqrt{4\,\lambda\,\xi'\,(\eta\;+\;L_0)}\right)\,. \tag{24}$$

Define

$$\omega_0 \,=\, \sqrt{4\,\lambda}\,; \qquad\qquad \tilde{Q}^2 = \sqrt{Q_1^2\,Q_2^2}\,.$$

The amplitude for $\gamma^*\,\gamma^*$ scattering is obtained using Eq. (20)

$$T^+ \,=\, T(Q_1^2,\,Q_2^2,\,s) \,=\, \frac{4\,\tau_{TT}}{\omega_0^2}\,\left[I_0\left(\omega_0\,\sqrt{\ln\frac{s}{Q_1^2}\,\ln\frac{s}{Q_2^2}}\right)\,-\,1\right] \quad if\;\; \mu_0^2 \,<\, \frac{\tilde{Q}^4}{s} \tag{25}$$

and

$$T^- = T(Q_1^2,\,Q_2^2,\,s) \,=\, \frac{4\,\tau_{TT}}{\omega_0^2}\,\times$$

$$\left[I_0\left(\omega_0\,\sqrt{\ln\frac{s}{Q_1^2}\,\ln\frac{s}{Q_2^2}}\right)\,-\,1-\,\frac{\ln\frac{s\,\mu_0^2}{\tilde{Q}^4}}{\ln\frac{s}{\mu_0^2}}\,I_2\left(\omega_0\,\sqrt{\ln\frac{s\,\mu_0^2}{\tilde{Q}^4}\,\ln\frac{s}{\mu_0^2}}\right)\right]$$

$$if\;\; \mu_0^2 \,>\, \tilde{Q}^4/s\,. \tag{26}$$

It is important to note that the final result for the amplitude is fully symmetric with respect to the photon virtualities. The amplitude T^- reduces to T^+ when $\tilde{Q}^4/s = \mu_0^2$, i.e. when the dynamical infrared cutoff of the perturbative calculation reaches μ_0^2, the limit of the nonperturbative infrared region.

Let us consider, in some more detail, the $s \,\to\, \infty$ asymptotics for the case $Q_1^2 \,\simeq\, Q_2^2 \,\gg\, \mu_0^2$. We take s to be much larger than the Q_i^2, but still within the region I^+ (9):

$$1 \ll s/\tilde{Q}^2 \ll \tilde{Q}^2/\mu_0^2. \tag{27}$$

In this region the asymptotics is obtained from the asymptotic behavior of the Bessel function I_0

$$T^+(s\,\to\,\infty) \,=\, \frac{4\,\tau_{TT}}{\omega_0^2\,\sqrt{2\,\pi\,\omega_0\,\ln(s/\tilde{Q}^2)}}\,\left(\frac{s}{\tilde{Q}^2}\right)^{\omega_0}\,, \tag{28}$$

and the result is entirely perturbative. When s increases and eventually reaches the boarder line between I^+ and I^-: $s/\tilde{Q}^2 \,=\, \tilde{Q}^2/\mu_0^2$ we have to switch to T^-. With a further increase of s, initially, the second term in (26) is not large and we can use the expansion of the Bessel function I_2 for small arguments. In the asymptotic region

$$\tilde{Q}^2/\mu_0^2 \,\ll\, s/\tilde{Q}^2 \tag{29}$$

the arguments of both Bessel functions are large. The leading asymptotics cancel and we have to take into account first corrections. We obtain:

$$T^-(s\,\to\,\infty) = \frac{8\,\tau_{TT}}{\omega_0^2\,\sqrt{2\,\pi}\,(\omega_0\,\ln(s/\tilde{Q}^2))^{3/2}}\,\left(\frac{s}{\tilde{Q}^2}\right)^{\omega_0}\,\times \tag{30}$$

$$\left[1\,+\,\omega_0\,\ln\frac{\tilde{Q}^2}{\mu_0^2}\,+\,\frac{\omega_0^2}{4}\,\ln^2\frac{\tilde{Q}^2}{\mu_0^2}\,+\,O\left(\frac{\omega_0^4\,\ln^4\frac{\tilde{Q}^2}{\mu_0^2}}{\ln\frac{s}{\tilde{Q}^2}}\right)\right]\,.$$

It is interesting to compare (28) and (30): the power behavior in s is the same in both regions. The difference lies in the preexponential factors: in the second region, we have a slightly stronger logarithmic suppression, and there is a logarithmic dependence upon the infrared scale μ_0^2.

Another case of interest is deep inelastic scattering on an almost real photon at very small x. This corresponds to the limit $\mu_0^2 \approx Q_2^2 \ll Q_1^2 \ll s$, and only the region I^- applies ($Q \equiv Q_1$) with $T_{DIS}(Q^2, s)$ given by Eq. (26). The Bjorken x is defined in a standard way: $x \equiv Q^2/s$. The flavor nonsinglet photon structure function is related to T_{DIS} via

$$F_{NS}^{\gamma}(x, Q^2) = \frac{Q^2}{4\,\pi^2\,\alpha_{em}}\,\sigma_{tot}^{\gamma^*\gamma} \simeq \frac{x}{4\,\pi\,\alpha_{em}}\,\frac{\partial\, T_{DIS}(Q^2, s)}{\partial \ln s}\,. \tag{31}$$

We can consider two different asymptotic limits. The first one is $\ln 1/x \gg \ln Q^2/\mu_0^2 \gg 1$. In this limit the structure function becomes:

$$F_{NS}^{\gamma}(x, Q^2) \simeq \left(\frac{1}{x}\right)^{-1\,+\,\omega_0}\,\frac{2\,\tau_{TT}\,(\,1\,+\,\omega_0\,\ln(Q^2/\mu_0^2)/4\,)^2}{\alpha_{em}\,\omega_0^2\,\sqrt{2\,\pi\,\omega_0}\,\ln^{3/2}(1/x)}\,\left(\frac{Q^2}{\mu_0^2}\right)^{\omega_0/2}\,. \tag{32}$$

Eq. (32) gives the Regge limit of the flavor nonsinglet structure function. Up to the preexponential factor this result agrees with the behavior of the flavor nonsinglet proton structure function found in [15,21].

Another asymptotic limit to be considered is $1 \ll \ln(1/x) \ll \ln(Q^2/\mu_0^2)$ leading to

$$F_{NS}^{\gamma}(x, Q^2) \simeq x\,\frac{\tau_{TT}}{\alpha_{em}\,\pi\,\omega_0^2\,\sqrt{2\,\ln(1/x)\,\ln(Q^2/\mu_0^2)}}\,e^{\,\omega_0\,\sqrt{\ln(1/x)\,\ln(Q^2/\mu_0^2)}}\,. \tag{33}$$

Eq. (33) comes from the asymptotic expansion of the first term in (26). The second term is subleading in this limit. Eq. (33) corresponds to the double logarithmic limit of the DGLAP equation.

4. The phase space of the double logs

It is instructive to compare our results for the high energy behavior of quark-antiquark exchange in $\gamma^*\gamma^*$ scattering with those for gluon exchange, i.e. the LO BFKL Pomeron. For the latter it is well-known that, for sufficiently large photon virtualities and not too high energies, the internal transverse momenta are of the order of the photon virtualities and hence justify the use of perturbation theory (Fig. 3a). When energy grows, diffusion in $\ln k^2$ (neglecting the running of α_s) broadens the relevant region of internal transverse momenta, which has the shape of a "cigar". Its mean size is of the order $\sqrt{\ln s}$ and eventually reaches the infrared cutoff μ_0^2. If energies increases further, the BFKL amplitude - although infrared finite - becomes sensitive to infrared physics, and some modification has to be included in order take care of nonperturbative physics.

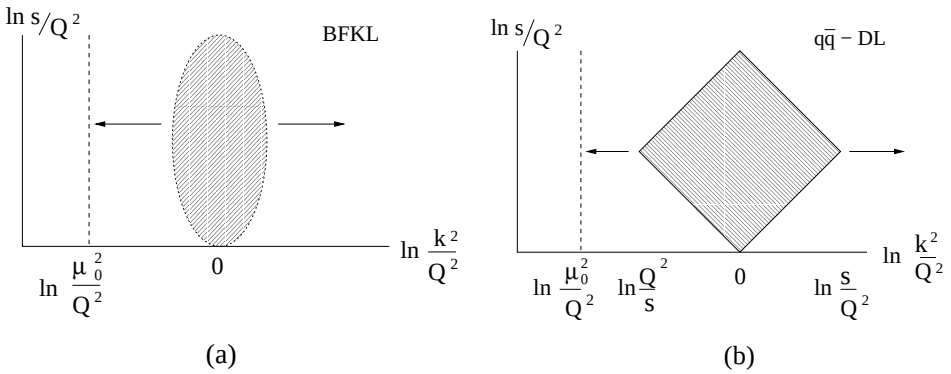

Fig. 3. Energy dependence of the region of integration in a) BFKL and b) quark ladder.

With the results of our analysis we now can make an analogous statement about quark-antiquark exchange. Since internal transverse momenta range between $max(Q^4/s,\, \mu_0^2) \,<\, k^2 \,<\, s$ or, equivalently

$$max(-\ln s/Q^2,\, \ln\, \mu_0^2/Q^2) \;<\; \ln\, k^2/Q^2 \;<\; \ln\, s/Q^2\,, \tag{34}$$

there is, for not too large energies, again, a limited region where transverse momenta stay above the infrared scale, and the use of perturbative QCD is justified. With increasing energy, the k^2-region expands and eventually hits the infrared cutoff μ_0^2. From now on the high energy behavior starts to depend upon infrared physics and requires suitable modifications.

In order to understand, in the fermion case, the region of internal integration in more detail, let us first return to our amplitude, A^+ (illustrated in Fig.2). It satisfies the two dimensional wave equation (22). It is instructive to introduce the new variables

$$t \,=\, \frac{1}{2}\,(\xi \,+\, \eta) \,=\, \ln \frac{\beta s}{\sqrt{k^2 Q^2}}\,; \qquad\qquad z \,=\, \frac{1}{2}\,(\eta \,-\, \xi) \,=\, \frac{1}{2}\,\ln \frac{k^2}{Q^2}, \tag{35}$$

which leads to the two-dimensional Klein-Gordon equation:

$$\left(\frac{\partial^2}{\partial t^2} \,-\, \frac{\partial^2}{\partial z^2} \,-\, 4\,\lambda\right)\, A^+ \,=\, 0 \tag{36}$$

(here $i\sqrt{4\,\lambda}$ plays the role of the mass).

Let us confront this with the BFKL Pomeron: in Fig.3b we have drawn the square which illustrates the internal region of integration. Apart from the difference in shape ("diamond" versus "cigar"), the most notable difference is the width in $\ln k^2$. In the fermion case it grows proportional to $\ln\, s/Q^2$, i.e stronger than in the BFKL case where $\ln\, k^2$ grows as $\sqrt{\ln\, s/Q^2}$: the BFKL diffusion is replaced by a linear growth in the z-direction. Also the definition of 'internal rapidity' is different: in the BFKL case the vertical axis can be labeled simply by $\ln\, 1/\beta$, whereas in the

fermion case our variable is $t = \ln(\beta s/\sqrt{k^2 Q^2})$ (in both cases, the total length grows proportional to $\ln s$).

5. Numerical estimates

The final goal of this project should be a confrontation of the obtained results with the LEP data. We are not ready yet to produce such a comparison since we still miss a significant theoretical contribution arising from the flavor nonsinglet exchange. In this section we will present some first numerical estimates related to the resummation of the quark ladder.

Using Eq. (13) the flavor nonsinglet contribution to $\sigma_{tot}^{\gamma^*\gamma^*}$ can be computed from the elastic amplitude (25) and (26). In our numerical estimates we will drop the flavor factor F_{ns}: the missing flavor singlet piece will be estimated to have the same functional form as the nonsinglet piece, and (13) - with the factor F_{ns} being replaced by $\sum e_q^4$ - is assumed to represent the sum of flavor singlet plus flavor nonsinglet.

First let us demonstrate numerically the effect of the two kinematical regions appearing in (25) and (26). Fig. 4 shows the $\gamma^*\gamma^*$ cross section as a function of rapidity $Y = \ln s/Q^2$ for equal masses $Q_1^2 = Q_2^2 = Q^2 = 16\,GeV^2$. Up to $Y \simeq 6$ this corresponds to the LEP data region. For the fixed value of α_s we use $\alpha_s(Q^2) \simeq 0.24$. The three curves show the dependence of the cross section on the nonperturbative scale μ_0. The solid line shows the (unphysical) case $\mu_0^2 = 0$ (the region I^+), the dotted line is $\mu_0^2 = 0.5\,GeV^2$, and the dashed line is $\mu_0^2 = 1.2\,GeV^2$. The points where the different curves come together correspond to $s\,\mu_0^2/Q^4 = 1$. To the left of these points we have the hard domain where the perturbative QCD calculation is fully reliable and does not depend upon the infrared scale μ_0^2. Note that for $\mu_0^2 = 0.5\,GeV^2$, almost all LEP data are within the hard domain. In this region we should expect that the secondary reggeon contribution is described by pQCD, and one should not add a further nonperturbative reggeon.

Fig. 5 compares the ladder resummation with the box diagram contribution[a]. A significant enhancement is observed. The enhancement grows at higher energies and reaches a factor of ten at $Y \simeq 10$. For comparison we also show the nonperturbative reggeon (dashed line) $\sim s^{-0.45}$. In Ref. [7] this contribution was added to the box diagram in order to fit the data. We believe that within the hard domain our resummed ladder should replace the contribution of the phenomenological reggeon. This can be qualitatively seen from the Fig. 5.

6. Conclusions

In this letter we have considered quark-antiquark exchange in $\gamma^*\gamma^*$ scattering. A closed expression for the cross section $\sigma^{\gamma^*\gamma^*}$ in the flavor nonsinglet channel is

[a] Only the leading logarithmic contribution is taken for the box diagram. The results thus obtained are somewhat larger compared to the ones based on the exact expression for the box.

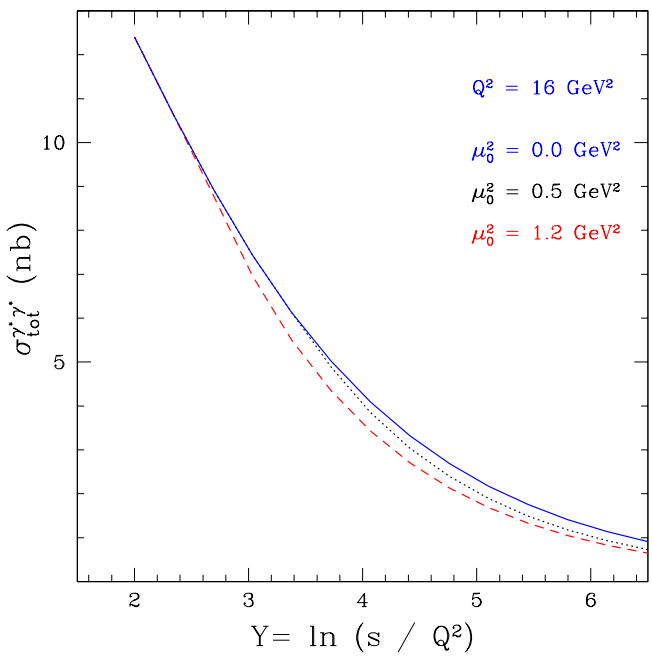

Fig. 4. $q\,\bar{q}$ contribution to $\sigma_{tot}^{\gamma^*\gamma^*}$ for various values of μ_0^2.

given. The result is valid within the double logarithmic accuracy of pQCD. The cross section depends on the four scales relevant for the problem $s \gg Q_1^2 \geq Q_2^2 \geq \mu_0^2$.

The resummed quark ladder serves as a model for a 'perturbative secondary reggeon'. It is remarkable that the resulting intercept $\omega_0 \sim 0.5$ is very close to the one known from the high energy phenomenology. The large intercept is due to the fact that the leading contribution is double logarithmic and $\omega_0 \sim \sqrt{\alpha_s}$.

One of the main observations is the role of the infrared cutoff μ_0 introduced into the analysis as the momentum scale below which perturbative physics is not reliable. For a given energy and for large photon virtualities Q_1^2, Q_2^2, we found that all the internal transverse momenta lie in the hard region. For this kinematics the result does not depend upon the infrared cutoff and the perturbative analysis is reliable. When energy increases beyond the value $s = Q_1^2 Q_2^2/\mu_0^2$, the region of integration penetrates into the infrared domain and the results starts to depend upon μ_0^2. We show, however, that this dependence is logarithmically weak. Another interesting observation is the role played by μ_0^2 in setting the asymptotic high energy behavior of the amplitude. Quite in analogy with the non-forwardness t of the BFKL physics, the appearance of μ_0^2 modifies the pre-exponential behavior of the asymptotics.

The study of the quark ladder has an obvious phenomenological motivation. The LEP data on $\gamma^*\,\gamma^*$ are at energies at which the quark box still gives a dominant

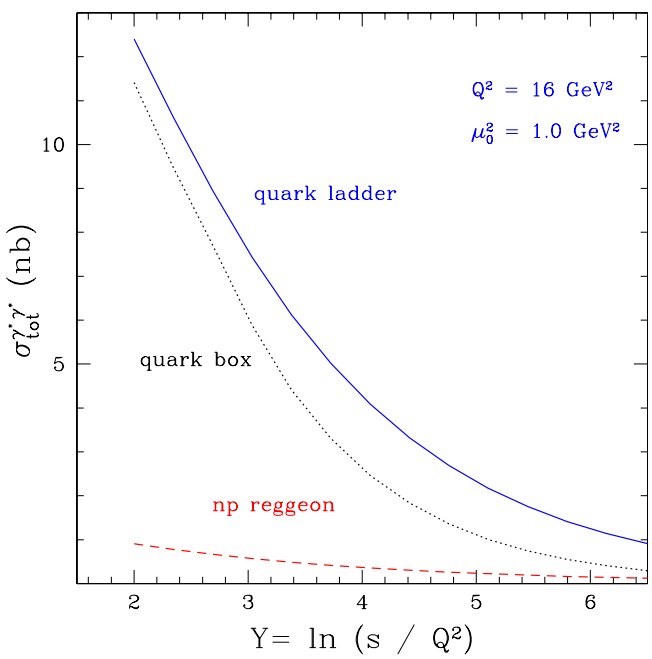

Fig. 5. Various contributions to $\sigma_{tot}^{\gamma^*\gamma^*}$.

contribution to the cross section. We have shown that the gluon radiation leads to a significant enhancement of the quark box and hence needs to be accounted for. The quark box contribution dies fast with energy and is correctly expected to be of no importance for $\gamma^*\gamma^*$ scattering at a NLC. In contrast, the pQCD reggeon receives an enhancement of about a factor of ten compared to the quark box, and potentially can still give a noticeable correction to the dominant pomeron contribution.

We have derived the low-x asymptotics of the DIS flavor nonsinglet photon structure function. The power dependence on x is shown to be the same as for the proton structure function [15,21].

In the double logarithmic approximation, the intercept of the $q\bar{q}$ system comes out large. Hence it will be important to investigate corrections to this leading order result. First corrections will come from the single logarithmic contributions of the ladder graphs. While the intercept does not acquire a single logarithmic correction [18] there is a hope that residue corrections could be computed from the reggeon Green's function approach [19]. The influence of the running strong coupling constant is another important aspect expected to come in at the level of NLO corrections. Qualitatively, the running coupling enhances the importance of the low momentum region.

From the phenomenological point of view our analysis is incomplete. We have

not yet calculated the flavor singlet quark-antiquark exchange which involves an admixture of t-channel gluons.

Acknowledgments

We wish to thank Boris Ermolaev, Victor Fadin, Dima Ivanov, Roland Kirschner, Genya Levin, Lev Lipatov, Misha Ryskin, Anna Stasto, and Lech Szymanowski for very fruitful discussions.

This research was supported in part by the GIF grant # I-620-22.14/1999.

References

1. E. A. Kuraev, L. N. Lipatov, and F. S. Fadin, *Sov. Phys. JETP* **45** 199 (1977) ; Ya. Ya. Balitsky and L. N. Lipatov, *Sov. J. Nucl. Phys.* **28** 22 (1978).
2. P. Achard *et al.* [L3 Collaboration], *Phys. Lett.* **B 531** 39 (2002).
3. G. Abbiendi *et al.* [OPAL Collaboration], *Eur. Phys. J.* **C 24** 17 (2002).
4. S. J. Brodsky, F. Hautmann and D. E. Soper, *Phys. Rev.* **D 56** 6957 (1997).
5. J. Bartels, A. De Roeck and H. Lotter, *Phys. Lett.* **B 389** 742 (1996).
6. A. Donnachie, H. G. Dosch and M. Rueter, *Eur. Phys. J.* **C 13** 141 (2000); *Phys. Rev.* **D 59** 074011 (1999).
7. J. Kwiecinski and L. Motyka, *Eur. Phys. J.* **C 18** 343 (2000).
8. N. N. Nikolaev, J. Speth and V. R. Zoller, *J. Exp. Theor. Phys.* **93** 957 (2001), [*Zh. Eksp. Teor. Fiz.* **93** 1104 (2001)].
9. S. J. Brodsky, V. S. Fadin, V. T. Kim, L. N. Lipatov and G. B. Pivovarov, *JETP Lett.* **76** 249 (2002), [*Pisma Zh. Eksp. Teor. Fiz.* **76** 306 (2002)]; hep-ph/0111390.
10. M. Cacciari, V. Del Duca, S. Frixione and Z. Trocsanyi, *JHEP* **0102** 029 (2001).
11. M.G. Ryskin and A.G. Shuvaev, *Eur. Phys. J.* **C 25** 245 (2002).
12. V. G. Gorshkov, V. N. Gribov, L. N. Lipatov and G. V. Frolov, *Sov. J. Nucl. Phys.* **6** 95 (1968), [*Yad. Fiz.* **6**, 129 (1967)]; *Sov. J. Nucl. Phys.* **6** 262 (1968), [*Yad. Fiz.* **6** 361 (1967)].
13. R. Kirschner and L. N. Lipatov, *Nucl. Phys.* **B 213** 122 (1983). *Sov. Phys. JETP* **56** 266 (1982), [*Zh. Eksp. Teor. Fiz.* **83** 488 (1982)].
14. J. Bartels and M. Lublinsky, *JHEP 0309* 076 (2003).
15. B. I. Ermolaev, S. I. Manaenkov and M. G. Ryskin, *Z. Phys.* **C 69** 259 (1996).
16. J. Bartels, B. I. Ermolaev and M. G. Ryskin, *Z. Phys.* **C 72** 627 (1996).
17. J. Bartels, B. I. Ermolaev and M. G. Ryskin, *Z. Phys.* **C 70** 273 (1996).
18. J. Kwiecinski, *Phys. Rev.* **D 26** 3293 (1982);
    R. Kirschner, *Z. Phys.* **C 31** 135 (1986).
19. R. Kirschner, *Z. Phys.* **C 67** 459 (1995).
20. V. M. Budnev, I. F. Ginzburg, G. V. Meledin and V. G. Serbo, *Phys. Rept.* **15** 181 (1974).
21. M. Lublinsky, *Phys. Rev.* **D 69** 077502 (2004).